

Document downloaded from:

<http://hdl.handle.net/10251/59886>

This paper must be cited as:

Desantes Fernández, JM.; Pastor, JV.; García Oliver, JM.; Briceño Sanchez, FJ. (2014). An experimental analysis on the evolution of the transient tip penetration in reacting Diesel sprays. *Combustion and Flame*. 161(8):2137-2150.
doi:10.1016/j.combustflame.2014.01.022.



The final publication is available at

<http://dx.doi.org/10.1016/j.combustflame.2014.01.022>

Copyright Elsevier

Additional Information

Elsevier Editorial System(tm) for Combustion and Flame
Manuscript Draft

Manuscript Number: CNF-D-13-00376R2

Title: An experimental analysis on the evolution of the transient tip penetration in reacting Diesel sprays

Article Type: Accepted Paper

Keywords: Fuel-air mixing, Diesel combustion, autoignition, lift-off length, schlieren, reacting tip penetration, diffusion flames

Corresponding Author: Dr. Jose Maria Garcia-Oliver, Ph.D.

Corresponding Author's Institution: Universitat Politècnica de València

First Author: JOSE M DESANTES, Prof.

Order of Authors: JOSE M DESANTES, Prof.; JOSE V PASTOR SORIANO, Prof.; Jose Maria Garcia-Oliver, Ph.D.; FRANCISCO J BRICEÑO

Manuscript Region of Origin: SPAIN

An experimental analysis on the evolution of the transient tip penetration in reacting Diesel sprays

José M. Desantes, José V. Pastor, José M. García-Oliver and Francisco J. Briceño

Abstract

Schlieren imaging has helped deeply characterize the behavior of diesel spray when injected into an oxygen-free ambient. However, when considering the transient penetration of the reacting spray after autoignition, i.e. the Diesel flame, few studies have been found in literature. Differences among optical setups as well as among experimental conditions have not allowed clear conclusions to be drawn on this issue. Furthermore, soot radiation may have a strong effect on the image quality, which cannot be neglected.

The present paper reports an investigation on the transient evolution of Diesel flame based upon schlieren imaging. Experimental conditions have spanned values of injection pressure, ambient temperature and density for typical Diesel engine conditions. An optimized optical setup has been used, which makes it possible to obtain results without soot interference. Based on observations for a long injection event (4 ms Energizing Time), the analysis has resorted to extensive comparison of inert and reacting sprays parameters, which have made it possible to define different phases after autoignition.

Shortly after autoignition, axial and radial expansion of the spray have been observed in terms of axial penetration and radial cone angle. After that, during a stabilization phase, the reacting spray penetrates at a similar rate as the inert one. Later, the reacting spray undergoes an acceleration period, where it penetrates at a faster rate than the inert one. Finally, the flame enters a quasi-steady penetration phase, where the ratio of reacting and inert penetration stabilizes at a nearly constant value. The duration of the reacting spray penetration stages shows modifications when varying engine parameters such as air temperature, air density, injection pressure, and nozzle diameter. However, the proportionality between reacting and inert penetration has been observed to depend mainly on temperature, in agreement with observed reductions in entrainment when shifting from inert to reacting conditions.

1 Introduction

Throughout the years, transient injection and combustion phenomena within direct injection diesel engines have been widely studied to optimize engine combustion and emissions. Part of this research effort has been performed by means of optical techniques, which has produced a deep understanding of fundamental processes that have been summarized in conceptual models, such as the ones by Dec [1] or more recently by Musculus et al. [2].

Such investigations have confirmed the fundamental role of fuel-air mixing process over the combustion process. The usual approach for the research community to undertake spray mixing studies has been by decoupling it from the combustion process by using singular test rigs that reproduce engine thermodynamic conditions in an oxygen-free atmosphere [3-6]. Such non-reacting studies have been focused on the detailed description of quantitative spray parameters, such as vapor spray tip penetration, liquid length, or local equivalence ratio. Classical examples are those by Naber and Siebers [7], which have provided non-reacting penetration data in a wide range of gas densities (from 3.3 kg/m^3 to 58.6 kg/m^3) and air temperature values (from 600 to 1400K). More recent works [8] confirm that current knowledge of spray flow evolution under inert conditions is quite deep.

On the other hand, there is also a wealth of information of spray processes under reactive conditions, but most of it is devoted to particular phenomena such as autoignition [9], lift-off length [10,11] or soot formation within the diffusion flame [12-16]. Compared to the detailed knowledge of inert spray flow, much less information is available in the literature on the evolution of the spray flow during the ignition and subsequent flame development. This lack of knowledge has even led to some phenomenological models to use a description of the penetration process under inert conditions even after the start of combustion [17].

A first study reported by Kobayashi et al. [18], where the reacting spray tip penetration was investigated in a rapid compression machine by means of the schlieren technique under thermodynamic conditions characteristic of low engine load (17.2 kg/m^3 density and 627 K temperature), showed for a long injection event (3.8 ms duration) a similar evolution of the spray tip penetration previous to the autoignition process (2 ms) when compared to the non-reacting spray. Soon after the autoignition, they found a slight increase on the spray tip penetration that progressively decreased during the injection event to even penetrate slower than the non-reacting case near the End Of Injection (EOI). Siebers [19] extended the data based in [7] and showed that the reacting spray behavior compared to the inert one depends on ambient density. Penetration was found to be similar to the non-reacting case for the lowest density values due to a long ignition delay, which was similar to observations by Kobayashi [18]. However, as density increased (i.e. shorter ignition delay), the spray penetration began to deviate from the non-reacting case, with a faster progression that could be observed until the EOI.

Pickett and Hoogterp [20] investigated reactive spray penetration with schlieren imaging under moderate EGR conditions ($15\% \text{O}_2$; 22.8 kg/m^3 ambient density and 900 K ambient temperature) for a 1.5ms injection event. Similar trends were observed during the autoignition and later penetration phases as reported by Siebers in [19]. Additionally, they observed a strong radial expansion at the time when tip penetration detaches from the non-reacting case, which also was coincident in time with the sudden increase of the soot luminosity recorded with a photodiode. Close to the EOI, they found that the tip penetration was similar to the penetration of the non-reacting case.

Finally, preceding work by Desantes et al. [21] made use of a 1D spray model developed in [22] to identify some of the processes occurring during the spray autoignition and subsequent flow penetration. Model predictions were compared to experimental measurements from an optical engine run at a 29 kg/m^3 density and 780 K temperature for injection duration of 1.3 milliseconds. Despite the experimental test matrix is somewhat limited and optical window size did not allow to fully visualize the stabilized flame, the spray

width is observed to increase after autoignition, and momentum flux along the spray changes abruptly compared to the inert case, where radially integrated momentum flux is conserved along the spray. The flow reacts in the direction of increasing local velocities, and therefore penetration rate, up to a point where momentum flux is re-balanced, and the flame penetrates as a zero-delay one.

From the above findings, spray tip penetration after autoignition seems to increase over the inert case at a rate somewhat depending on the test conditions. Different experimental results show that sometimes there is a clearly faster penetration, while in other cases differences between inert and reacting spray tip evolution are within the experimental uncertainty. Given the fact that different schlieren optical arrangements were used in previous investigations [18-21], a question can be raised as to how strong the influence of the setup on the results can be or, if this behavior is mainly dependent on the operating conditions.

The present paper tries to contribute to the understanding of the transient effects induced by combustion on the spray penetration and the flow evolution. In agreement with preceding works and also with literature reports, schlieren imaging of the reactive spray evolution will be performed. Careful considerations presented in [23] have been accounted for when setting up the system optics to enable reliable schlieren measurements. Tests have been performed in a Constant-Pressure Flow (CPF) vessel with a much larger visualization system than in [21]. A wide set of conditions has also been investigated to try to evaluate the validity of previous conclusions. Finally, analysis has considered not only spray penetration, but also increase in radial width, and lift-off length measurements. The reported free spray results, with maximum tip penetration in the range of 100 mm, are not intended to be extrapolated to a real engine, where wall distance to the nozzle is typically below 50 mm. However, processes governing tip penetration within the reported experiments should be similar to those within an engine spray. Accordingly, the purpose of the paper is the gaining of fundamental knowledge to understand such phenomena.

The manuscript is structured as follows: Right after this introduction, the experimental facility, optical configuration and processing routines are described. Then, the different operating conditions covered in this investigation are presented. Analysis of results has been divided into four different subsections. Starting from a general description, the transient evolution of the reacting spray is defined as well as the parameters used for further parametric analysis. After that, considerations for reacting spray 1D modeling in terms of reacting spray angle significance are detailed. Next, a statistical evaluation of Lift-Off Length (LOL) measurements from schlieren images is performed enabling interpretation of the reacting penetration behavior through evaluation of the fuel-air mixtures upstream the LOL. Lastly, the influence on the global description of the transient flame evolution of some of the most relevant operating variables (namely injection pressure, air temperature, air density and nozzle diameter) is evaluated. The conclusions section summarizes the most important finding of this paper.

2 Experimental apparatus

Experiments have been conducted in an optically accessible Constant Pressure Flow vessel (CPF). Gas within this facility can be pressurized and heated up to 15 MPa and 1000 K, respectively. The facility can be operated in either open or closed loop. In the former case, dry fresh atmospheric air is supplied by a volumetric compressor. In closed loop operation, N₂/O₂ mixtures at controlled composition are re-circulated along the circuit, reproducing non-reacting ([O₂] = 0%) or EGR conditions.

The gas velocity across the chamber has been estimated to be minor compared to the spray velocities even at far distances from the spray tip, with approximate values of 0.2 m/s and 0.4 m/s. As a consequence, a quasi-quiescent environment is obtained, and the shot-to-shot spray dispersion is reduced when compared to optical engines and rapid compression machines. Since high temperatures are continuously sensed on the injector tip, a water coolant circuit has been drilled in the injector port in order to maintain a user-selected

constant and safe temperature on the injector body. An independent electronic system permits to establish the injection frequency during the experiments, being 0.5 Hz for this investigation.

Four orthogonally drilled ports provide access to the combustion chamber. The first of these accesses is occupied by the injector port and the cooling system for the injector body. The other three accesses are equipped with round quartz windows (128 mm in diameter) in a T-shaped path providing both perpendicular access and frontal view for spray analysis of single-hole nozzles and multiple-hole nozzles, respectively.

3 Schlieren imaging

Based upon the spatial variation of the refractive index of target liquids or gases [24], schlieren is a common technique to evaluate the vapor phase fuel evolution in hot ambient gases such as in test rigs for Diesel combustion investigation. The same arrangement as in previous works [23,25] has been used, namely a “focused single pass” schlieren setup, as sketched in *Figure 1*. This optical arrangement can be divided in two different sections, which are referred to as the illumination and collection sections. Upstream the spray on the illumination section, a coherent and parallel light ray array was created by placing a diffused point light source at the focal length of a parabolic mirror ($f=610$ mm). This diffused pointed source (iris clear aperture of 2 mm) has been obtained by integration of the light coming out of a Xenon arc lamp through a liquid light guide and orienting the light orthogonally to the vessel. The visualization area was maximized because of the mirror diameter (150 mm) being larger than the optical windows (128 mm).

Downstream the spray on the collection section, the schlieren phenomenon takes place due to the deviation of the light rays from their original path (i.e. beam steering [15]) because of the density gradients between the fuel (liquid or vapor) and the hot ambient gases. The label “focused” of this technique comes from the need of concentrating both deviated and un-deviated rays into a small area such as the camera pixel array. That is why a spherical lens is placed after the combustion vessel that helps concentrating the light onto the so-called Fourier plane. The camera (Vision Research Phantom V710) is placed right after this plane together with a commercial lens that finally drives all the shadowgraph onto the camera sensor. *Table 1* shows the image size and conversion mm-pixel resulting from this optical arrangement, as well as, the frame rate and exposure time set on the high-speed camera.

In previous works authors have investigated about the uncertainties and limitations on the particular schlieren optical set-up [25] as well on the final digital analysis and measurements [23]. In that sense, particularities on the collection section are briefly recalled here in order to empathize the fact of having a “controlled” schlieren system. Placing the spherical lens (see *Figure 1*) right after the vessel window helped maximize the collection angle leading to a fully controlled filtering on the Fourier plane despite the expected rays clipping because of (i) the long distance between the spray focused plane and the collecting spherical lens (~ 300 mm) and (ii) because a finite size of the collecting lens (diameter=150 mm). The spatial filtering set on the Fourier plane with an iris clear aperture of 4 mm helped maximize the schlieren sensitivity of high diluted fuel in air when performing inert tests. Furthermore, for reacting tests it also helped minimize or even eliminate the high luminosity from soot radiation. Together with the spatial filter, chromatic filtering near the Fourier plane with a BG-39 (used as a bandpass filter, with a peak transmissivity of 88% at 513 nm; transmissivity is below 10% for wavelengths below 330 nm or above 660nm) and short exposure times of $0.3 \mu\text{s}$ on the camera sensor was adopted in this investigation. The final setup enabled the recording of images without strong soot radiation influence. This fact is highly desirable for image digital analysis avoiding artificial pixel saturation, i.e. blooming phenomena [26] on Diesel-like flames (further details on digital analysis can be found in [23]).

3.1 Spray tip penetration measurement

An open code for spray penetration measurements posted by the Engine Combustion Network (ECN) [27,28] has been used for tip penetration measurements. This code was developed by the Sandia National Laboratories group and can be found online [27]. The underlying algorithm tries to remove the schlieren effect of the hot ambient gases in order to more easily visualize the jet structure [29]. The code is based on the texture that a schlieren image I_t has at any time instant. A first temporal derivative process is performed to the image subtracting the two preceding images I_{t-1} and I_{t-2} . This process brings out the activity zones of the schlieren image, i.e. those pixels that experiment any change because of the spray motion (target measurement). Then, a second spatial standard deviation filtering is performed to 3x3 pixels region on the image, to remove the background hot-ambient gases motion from target sprays. Because of the already commented slow gas velocities in experimental apparatus such as the one used on this study (0.2-0.4 m/s), the expected maximum displacement of the background gases is approximately 1-pixel/40-images at the framing rates used in this investigation (see **Table 1**). Therefore background movement was proven to have no influence on the final result. The resulting image is treated for connectivity and the contour of the flame is established then, the penetration is measured following the procedure established in [7]. This parameter has been quantified for both inert (S_i) and reacting (S_r) ambient conditions.

3.2 Schlieren lift-off length location

As stated in the Introduction section, a radial cross-section increase due to combustion-induced expansion has been observed during the spray autoignition process that lasts along the premixed and diffusive combustion stages. The inert and reacting parts of the jet/flame meet at the Lift-Off Length (LOL) location, which is usually measured from OH* chemiluminescence images [30]. Indeed, the LOL was proven to coincide on the region where schlieren reacting contours depart from the inert contours as observed in **Figure 2**. A processing routine to calculate the lift-off length in a flame schlieren image (LOL_s) has been developed. This routine comprises the following steps (further details can be found in [23]).

1. A reacting spray contour is detected by a processing routine.
2. A cone shape contour is fitted to the initial inert part of the spray by means of a least-squares algorithm (top of **Figure 2**). This initial inert part is defined by the 80% of a user-defined initial estimation of the lift-off length.
3. At each location along the spray axis (X), the cross-sectional difference ΔR between the detected reacting sprays and the inert fitted contour is computed ($\Delta R = R_{\text{react}} - R_{\text{non-react}}$).
4. **Figure 2** shows the evolution of ΔR along the spray axis in non-dimensional units, ($\Delta R/\Delta X$, where ΔX is the pixel length). Along the near-nozzle inert part of the spray $\Delta R/\Delta X$, is approximately zero. On the reacting part, $\Delta R/\Delta X$ first increases to a maximum and then, progressively decreases to zero. Schlieren lift-off length (LOL_s) was defined as the distance from the nozzle to the location where this $\Delta R/\Delta X$ is 25% of the maximum value.
5. This process is repeated for both upper and lower contours and LOL_s in **Figure 2** represents the average value.

4 Operating conditions

Table 2 summarizes the target operating ambient pressures and temperatures set on the CPF vessel during the test campaign. Starting from a nominal condition, which has been labeled as **NO**, with 21.2 kg/m³ density and 826 K temperature, the study comprises five different ambient conditions with a density sweep at constant temperature and a temperature sweep at constant density. Those five conditions will be referred hereafter as **NO** for the Nominal conditions, **LT** for the Low Temperature, **HT** for the High Temperature, **LD** for Low Density and, **HD** for the High Density. Oxygen concentration is 21%, so no EGR effects have been considered. In [31], fluctuations on the boundary operating condition have been addressed by an

analysis of the temporal and spatial field of bulk gas temperature across the vessel, which has been observed to vary in a $\pm 5\text{K}$ range for the spray A conditions (22.8 kg/m^3 and 900 K) of the ECN community [27,28]. Adopting such variations for this study due to a constant pressure flow and a not significant variation of the heat transfer rates in this large vessel volume, the bulk gas density is expected to vary up to $\pm 0.17\text{ Kg/m}^3$ along the test conditions.

For each temperature-density conditions, two common-rail single-hole nozzles and three different injection pressure values (**Table 2**) have been used. The Energizing Time (ET) was 4 ms for all operating conditions, which is long enough to enable autoignition and subsequent diffusion flame development. N-Heptane was used as the fuel injected on each test condition, where 5 injection cycles have been recorded.

5 Results

5.1 Experimental analysis of the transient flame penetration phases

Taking into account the spatial limitations imposed by the 105 mm effective visualizing area of the CPF vessel (distance from the nozzle tip to widows limit), the baseline condition for the analysis in this section has been selected as the case within the test matrix where the flame evolution can be observed for a longer period. In practice, this means an early ignition (high ambient temperature or density) and a slow spray development (low injection pressure, small diameter and high density). As a result, the combination of HT ambient conditions with 50 MPa injection pressure and small $d_0=82\text{ }\mu\text{m}$ was considered in this section. Although time scales longer than the End Of Injection (EOI) can be visualized for this condition, the analysis presented here is focused on the momentum-driven flame period before EOI rather than on the transient phase after EOI where effects such as entrainment waves [32] occur.

Figure 3 to **Figure 5** show the experimental information that can help identify the different stages on the spray flame transient evolution. **Figure 3** shows a representative image sequence of an entire injection event that can be found in a video file included in the digital version of this paper (Appendix A). Such images have been produced by combining inert and reacting instantaneous half-images. Detected contours have been overlaid to aid in the visualization. On the other hand, **Figure 4** (top) includes the time-resolved spray penetration for both inert and reacting sprays. Solid lines on the temporal evolution represent a temporal average behavior, upon which a \pm one standard deviation interval is shown by shaded areas. For this condition, the coefficient of variation (standard deviation of the sample divided by average value) is below 4% along the injection period and for both inert and reacting conditions, and similar results are obtained for other conditions

Tip penetration for an inert spray injected under constant injection and ambient boundary conditions can be described by Eq. 1:

$$S_i = k \cdot \sqrt{d_{eq} \cdot u_0 \cdot t} \quad \text{Eq. 1}$$

where d_{eq} is the equivalent diameter, u_0 is injection velocity, t is time after start of injection and k is a proportionality constant that can be related to the air entrainment rate [33]. Subsequent analysis will indicate that the ratio S_r/S_i is a convenient quantitative parameter to establish a comparison with the inert case, as well as for the understanding of some of the flame penetration stages. In particular, if the penetration of the reacting spray flame S_r follows a similar evolution as the inert spray, one can define

$$S_r = k_r \cdot \sqrt{d_{eq} \cdot u_0 \cdot t} \quad \text{Eq. 2}$$

with k_r also defining a constant that contains combustion-related information other than the influence of inert mixing process, e.g. the reduction in entrainment as a consequence of heat release [34]. Under such assumptions, the penetration ratio will be equal to a ratio of constant parameters $S_r/S_i = k_r/k$. Therefore the ratio of reacting vs. non-reacting spray penetration at every time step S_r/S_i has also been included at the

bottom part of **Figure 4** . Finally, **Figure 5** shows the time-evolution of the ratio of the reacting and inert spray cone angles θ_r/θ_i , as well as selected images of the HT conditions previously shown in **Figure 3**.

The temporal evolution of the reacting tip penetration has been found to undergo different stages as injection progresses. As expected, prior to the autoignition process the reacting case does not experiment any difference in tip penetration when compared to the non-reacting one, as observed on the 0.456 ms image in **Figure 3**. Inspection of schlieren images shows that the autoignition process takes place at approximately 0.604 ms denoted by the expansion of the spray. According to that, the reacting spray undergoes a sudden increase in the penetration as compared to the inert case, and the penetration ratio S_r/S_i reaches a local maximum value at 0.711 ms, what is obviously connected to the initial drop in local density and consequent expansion of the mixture [19]. After this initial peak in penetration, the reacting spray seems to decelerate, as observed by the fact that spray tip penetration tends to match that of the non-reacting spray at 1.391 ms. The penetration ratio may even fall below one, as seen in **Figure 4**. After this stabilization period, where no big differences can be observed in S_r/S_i scales, the reacting spray undergoes an acceleration phase, and it eventually detaches from the inert one. This acceleration process is also somewhat transient, as the penetration ratio S_r/S_i shows a steady increase in the 2 to 4 ms interval, and later stabilizes at a quasi-constant value for the rest of the injection event. It is during this final stage that the penetration under reacting conditions seems to obey a quantitative description according to Eq. 2.

Apart from the tip penetration, which is an evaluation of spray axial evolution, the analysis of the radial dispersion of the spray, which has been here quantified in terms of a spray cone angle, can produce relevant information for the analysis of the spray flame evolution. This parameter has been extensively used in many spray studies to characterize the inert spray radial spreading rate [8,25,32,35], in spite of some uncertainties related to the differences in definition among different groups and well-known limitations of the schlieren technique to objectively resolve the spray limit from a background flow [8]. Images in **Figure 5** enable the identification of a sharp contour for the reacting case. It is highly difficult to discern the real meaning of the contour limit in terms of density, velocity or mixture fraction limit values. However, taking into account that the same optical layout has been used for both inert and reacting conditions, the present study has defined a spray cone angle that can be compared to the inert one to have a semi-quantitative evaluation of the radial spread of the spray under reacting conditions. For the purposes of this investigation, both inert θ_i and reacting θ_r spray cone angles have been obtained. θ_i is defined as the angle between two straight lines obtained by least-squares fitting of the 80% length along the inert zone of the spray (which can be obtained from the LOL analysis in section 4.2). In a similar way, the reacting spray cone angle θ_r has been defined as the angle between two straight lines obtained by least-squares fitting to the reacting spray contour for axial distances just downstream of the lift-off length (LOL_s) to an axial distance equal to 80% the spray tip penetration. It must be noted that both upper and lower lines defining the spray cone angle will very often cross at a positive axial location, which makes it difficult to compare to the inert case, where they cross at essentially zero or even negative values (virtual spray origin). According to the previous definitions, one cone angle ratio θ_r/θ_i can be derived from every single image after start of combustion.

When accounting for the previously-defined stages it can be observed that, during the autoignition and stabilization period, the spray undergoes a radial expansion which is much higher than that observed in the axial direction. Based upon the average evolution from the recorded cycles, the maximum radial expansion factor is $\theta_r/\theta_i = 2.6$ in **Figure 5**. After that, θ_r/θ_i decreases with time towards a sort of stabilized value $\theta_r/\theta_i = 1.3$ that lasts until the EOI. One cannot overlook the scattering among different injections, which can be also observed in the single shot-to-shot values (gray symbols) in **Figure 5**. This scattering is especially strong (around 40% of mean values) during the initial stages, where some repetitions can be observed to reach a peak $\theta_r/\theta_i = 3.5$, while others result in a very low initial expansion, which peaks later (at approximately 1.4 ms) with θ_r/θ_i slightly above 2.0. However, the scattering is not as strong during the

acceleration period (around 10% of mean values), and the decreasing trend of θ_r/θ_i with time can be identified with a high degree of confidence.

The previous result indicates that maximum radial expansion in a reacting spray occurs during the initial combustion stages, and evolves with time in a generally decreasing trend towards a steady value. This is quite different from the inert case, where a quasi-steady spray cone angle can be defined. For the HT conditions presented in this section, the quasi-steady value is reached earlier than the quasi-steady penetration ratio (around 3 ms, compared to 4 ms, respectively).

The last final observation that is worth mentioning is the time evolution of the lift-off length LOL_s , which has been also included in **Figure 4** (top). After a slightly higher initial value at the very onset of combustion, which can serve as an evidence of the fact that combustion starts at the tip of the spray, a nearly constant LOL_s value is observed along the whole injection period. Compared to the other quantitative parameters, very little scattering is observed (compare average curve with single values). This steady value agrees with time-resolved lift-off length derived from high-speed broad-band chemiluminescence images in [31]. As the flame evolves during the acceleration phase, LOL_s remains at a quasi-steady level typical for reacting sprays in CPF vessels, where ambient gas dynamics are less influential in comparison to optical engines or rapid compression machines [5,18].

According to the different experimental evidences, the temporal evolution of the reacting spray can be defined in five stages as follows.

- I. *Non-reacting phase*, previous to autoignition, where the mixing processes take place.
- II. *Autoignition expansion phase*, where the spray volume suddenly increases (in axial and especially in radial direction) because of the onset of combustion.
- III. *Stabilization phase*: Where the reacting flow evolution does not progress faster than the inert case. If momentum is conserved, density drop due to combustion should result in a faster penetration of the spray. However, this is compensated by the strong initial increase in radial width. As a result, the reactive flow does not penetrate faster than the inert one.
- IV. *Acceleration phase*, where the reacting tip penetration progresses sensitively faster than the inert one, and eventually detaches from that of a non-reacting spray. During this period, the penetration ratio (S_r/S_i) increases steadily with time.
- V. *Quasi-steady flame phase*, where the tip penetration ratio reaches a steady value.

5.2 1D Spray modeling considerations on transient flame penetration

This section intends to complement the previous experimental information by means of results from the 1D spray model. Even though the model has a highly simplified approach for detailed combustion modeling, it can still give further evidence on the effect on heat release on transient flow evolution. **Figure 6** shows a comparison of spray penetration under both inert and reacting conditions, as well as the ratio of reacting to non-reacting penetration. Both experiments and model results have been considered. Experimental injection data as well as ambient conditions are input for the 1D model, which has been calibrated in the same way as in [8,25] by fitting spray cone angle so that experimental inert penetration is adequately predicted. Considering the degree of accuracy in the prediction of inert spray penetration with similar 1D models, recent approaches have shown that spatial distribution of mixture fraction is also adequate [8].

When calculating under reacting conditions, two critical parameters have to be provided to the model, namely the time for start of combustion and a reacting spray cone angle. In the case shown in **Figure 6**, the reactive cone angle has been determined in the same way as for the inert case, i.e. a comparison of experimental penetration with model predictions for different reacting cone angle values. Due to the fact that reacting penetration undergoes several stages, experimental results suggest that the calibration of the modeling angle should be performed during the final quasi-steady penetration phase, where the evolution

can be more accurately compared to that of an inert spray according to Eq 2. Calibration results indicate that a larger spray cone angle needs to be used in the reactive case ($\theta_r = 25.5^\circ$) compared to the inert one ($\theta_i = 22.5^\circ$). Even though the expansion ratio of the model cone angle inputs ($\theta_r/\theta_i = 1.13$) is well below experimental values for the quasi-steady phase ($\theta_r/\theta_i = 1.3$), this provides an additional evidence of the existence of an expansion process lasting during the final quasi-steady penetration phase.

On the other hand, the model start of combustion in **Figure 6** has been selected at the start of the acceleration period. Comparison of modeled and measured reacting penetration values shows that 1D model transition to reacting conditions is faster than in the experiments. In particular, the initial period between start of combustion and the acceleration phase cannot be captured by the model, and for this reason the model start of combustion is shifted later. This could be reasonably expected, as model chemistry is highly simplified. As already described, autoignition timing is user-defined, and there is a zero-delay transition in chemistry to a flame based on a Burke-Schuman approach. Therefore, the model considers a zero-delay transition between inert and full reacting local conditions. In terms of a progress variable, this would mean a step change from 0 to 1.

Under the previous considerations, the model can still identify the experimental acceleration period followed by a quasi-steady penetration (stages IV and V). Furthermore, the modelled axial penetration ratio (S_r/S_i), although shifted too early due to the very fast chemistry approach, shows a maximum value that is very similar to the experiments. Tip penetration predictions are therefore capturing the physics occurring during this phase.

In a detailed analysis of model results in preceding work [21], an inert spray was shown to penetrate with a constant cross-sectional momentum flux along the axis. At start of combustion, the inert-to-reacting transition creates a drop in local density (as well as an increase in spray cone angle) that produces an unbalance in momentum flux along the spray. The spray reacts in the direction as to accelerate the flow, and therefore the tip penetration rate. This launches the acceleration phase (IV) until momentum flux along the spray is re-balanced, which coincides with the transition to the quasi-steady flame penetration period (V).

Interestingly, the model shows a progressive decay in the penetration ratio. This can be understood by the fact that as the flame penetrates farther from the nozzle it becomes more diluted, and average density at the tip decreases towards air density, becoming closer to the inert case. This effect is not clearly observed in the experiments, probably because of the limited reaction rate, compared to the model, with which the experimental reacting spray evolves.

5.3 Lift-off Length measurements

Before going into the analysis of the parametric effects on transient flame evolution, this section presents the results of Lift-Off Length (LOL) measurements for the investigated conditions. Results in previous section have shown that LOL is steady with time from almost the very start of combustion. This has been observed for all operating conditions in the present study. Accordingly, the time-averaged value turns out to be representative enough to enable a relatively simple statistical analysis. Furthermore, this time-averaged value can be compared to the more conventional long-exposure OH* imaging, which is more often found in the literature [9]. For that purpose, LOL was averaged in the 2.5 ms to 4 ms ASOI for each of the operating conditions under investigation. A statistical fit was performed with a model of the type:

$$LOL[mm] = k \cdot u_0^a [m/s] \cdot T_{air}^b [K] \cdot \rho_{air}^c [kg/m^3] \cdot d_0^d [m] \quad (Eq.3)$$

which can be very often found in the literature [11,23,36,37]. This analysis extends the previous reports in [23], where only injection pressure and temperature variations have been reported. Obtained coefficients have been shown in **Table 3** as compared to a widely used reference [36], and to more recent results [37] obtained in a Diesel-like optical engine.

Parametric trends among different sources are obviously in agreement, namely LOL increases with increasing velocity and diameter, and decreasing temperature and density. However, the quantification of the sensitivity by means of the corresponding exponent shows some differences among data sources. This can be due to differences in the experimental test rigs and methodologies, as well as to the fact that schlieren has been used for LOL determination, while the more conventional OH* imaging has been used in all the other works. All in all, highest sensitivity of LOL is found with temperature, followed by injection velocity and density, and lowest by orifice diameter.

On the other hand, LOL has been identified as an important parameter for soot formation within Diesel flame, as it controls the amount of air entrained from the nozzle to the flame base [12]. That is why some authors have used semi-empirical equations [11] to estimate the cross-sectional equivalence ratio at the flame base to correlate with soot formation processes within the diffusion flame [38]. It is quite logical to assume that this entrainment should also have an effect on combustion development, at least during the initial combustion stages. Following that idea, quantification of the mixture composition at the flame base has been done within the present investigation. For that purpose, measured LOL values have been used together with the 1D spray model under inert conditions to quantify the equivalence ratio on the spray axis at the flame base ϕ_{LOL} [22]. **Figure 6** shows the axial distribution of equivalence ratio for the condition discussed in previous section, so that when coupled to the experimental penetration one can derive ϕ_{LOL} . Results will be used in the following section to analyze transient combustion evolution.

5.4 Effect of operating parameters on transient flame evolution

In this section, the previously defined sequence of events during the transient flame evolution is discussed for some of the conditions within the parametric study. Following the previous methodology, results will be mainly analyzed in terms of reacting vs. non-reacting penetration and angle ratios. Only cases where the full spray tip penetration stages can be observed within the optical window have been selected.

Effect of injection pressure:

Figure 7 shows results of a variation of injection pressure for the HT condition, which has been selected for the sake of consistency with the nominal condition previously analyzed. In terms of ignition delay, results show that increasing injection pressure has practically no effect on the ignition delay timing, as the initial peak in the penetration ratio is coincident for all three cases (slight changes occur in the range of 10 μ s, which cannot be observed in this plot). This is not the case when dealing with the combustion-induced spray expansion. Cone angle ratio shows that the initial expansion decreases with higher injection pressure. This effect could be explained from the mixture state at the start of combustion: the higher the injection pressure, the further away from the nozzle ignition occurs, and therefore the leaner the mixture is. This is consistent with the longer LOL scaling injection velocity exponents that has been shown in Section 7. 1D model results indicate that equivalence ratio on the axis at LOL decreases with injection pressure following the trend $\phi_{50}=4.1 > \phi_{100}=3.2 > \phi_{150}=2.6$. As a consequence, leaner mixtures result in lower expansions at the combustion onset.

Regarding the stabilization phase results show a decrease in the duration of the stabilization period with higher injection pressures, both in terms of penetration or spray cone angle ratio. Higher injection pressure results in a higher momentum flux into the reacting zone, and therefore a faster flame evolution should be observed. This is also the case during the acceleration phase in **Figure 7**. However, a remarkable result is that (S_r/S_i) during the final quasi-steady phase is very similar for all three injection pressure cases. This means that, during this final penetration stage, injection pressure has exactly the same effect upon penetration rate as for an inert spray, except for a proportionality factor. Considering the initial analysis of the inert and reacting penetration in Eqs. 1-2, this would mean that k_r should not depend on injection pressure.

Effect of ambient temperature:

Considering that previous analyses have been performed for the HT conditions, decreasing ambient temperature has a large effect on combustion development, which has been exemplified in **Figure 8**. There is an obvious increase in autoignition delay with decreasing temperature, which can be observed by the later location of the initial peak in the (S_r/S_i) curves. This fact leads to an ignition process that occurs farther downstream from the nozzle, as observed in LOL results, with a consequent leaning of the ready-to-burn mixture ($\phi_{HT}=4.1 > \phi_{NO}= 3.2 > \phi_{LT}= 2.05$) and a smaller expansion ratio at the start of combustion both in radial (θ_r/θ_i) and axial directions (S_r/S_i).

The subsequent stabilization interval before the acceleration phase is also longer with decreasing temperature, and for the lowest case (LT) it extends even after the end of injection. During the acceleration period, the rate of change of both the radial expansion and axial penetration ratios are quite similar for both HT and NO cases. However, there is a quite noticeable drop in the quasi-steady axial penetration ratio with decreasing temperature. This should not be due to differences in entrainment at the flame base, since the equivalence ratio (ϕ_{LOL}) estimations are fairly similar to those observed in the injection pressure parametric study. There is therefore a definite thermal effect upon the quasi-steady penetration phase which could be linked to the changes in entrainment as a result of combustion-induced temperature change [34]. Considering the initial analysis of the inert and reacting penetration in Eqs. 1-2, this would mean that k_r seems to depend on ambient temperature, and therefore on local flame temperature values.

Compared to the other two cases, the LT case exhibits a noticeable drop in penetration ratio below one in the 1 to 2.5 ms interval. After that, the initial peak and subsequent acceleration stages as defined by the tip penetration ratio are similar in evolution to the other NO-HT cases, albeit delayed in time and with a slower development due to the lower rate of the chemical reaction. Initial low temperature reactions can explain the initial drop in penetration ratio below one in the 1 to 2.5 ms interval, before the spray runs into the high temperature autoignition. Such reactions span a longer interval the lower the ambient temperature.

Effect of ambient density:

Parametric trends with density can be observed in **Figure 9**. There is a trend towards a slower combustion development with decreasing density due to the lower mixing rate. This can be observed by a later onset of combustion with decreasing density. Results of cone angle ratio indicate that initial expansion in radial direction is delayed with density change, but does not drop significantly. This would mean that mixture state at the start of combustion is relatively similar, which can be confirmed by equivalence ratio estimations at the LOL position, which are weakly dependent on density ($\phi_{HD}=3.5 > \phi_{NO}= 3.2 > \phi_{LD}= 2.82$) compared to previous parametric variations with injection pressure or temperature.

Results confirm that the stabilization period before the acceleration phase is also longer as ambient density decreases. Finally, during the acceleration period, variation of the penetration ratio (S_r/S_i) is also lower with decreasing ambient density. However, all three density cases seem to converge towards a very similar quasi-steady value. This means that, during this final penetration stage, density has exactly the same effect upon penetration rate as for an inert spray, except for a proportionality factor. Considering the initial analysis of the inert and reacting penetration in Eqs. 1-2 this would mean that k_r should not depend on ambient density.

Effect of nozzle diameter:

As shown in **Table 2**, the investigated test matrix included the same experimental conditions for 82 and 138 μm diameter nozzles. Due to the larger size in the latter case, spray length scales are increased, and the observation window only allows to discern the different phases in high temperature and high density cases (HT and HD, resp.). **Figure 10** shows an example of comparison of nozzle effects for the high temperature HT case. Ignition seems to be delayed later by around 200 μs for the larger nozzle, probably due to the

slower mixing process. This slower mixing is also demonstrated by the equivalence ratio at the LOL ($\phi_{138} = 6.8 > \phi_{82} = 4.1$). The larger nozzle, however, runs faster into the acceleration period, and seems to converge to a similar quasi-steady penetration ratio compared to the smaller nozzle. However, this is not the case when comparing high density HD cases, where no convergence is observed for the quasi-steady phase. There is an inherent limitation in the optical window size with the larger nozzle, which does not allow for a final conclusion to be drawn based on the consideration of more experimental conditions. As a consequence, more investigation in this direction is needed.

6 Conclusions

An experimental study on the transient evolution of a reacting Diesel spray has been reported. Experiments have been conducted in a constant pressure vessel under conditions similar to those found in the cylinder of an engine. High speed schlieren imaging has been performed with the objective of understanding the spray transition from inert to reacting conditions during the autoignition and subsequent flame evolution. Different quantitative parameters have been derived from schlieren images, namely spray tip penetration, cone angle increase or lift-off length. From the first two, reacting-to-inert ratios have been used to quantify combustion-induced changes within the spray both in axial (S_r/S_i) and radial (θ_r/θ_i) directions.

The experimental analysis of high-speed transient schlieren images together with 1D spray model predictions have provided relevant information to determine the different stages of the macroscopic spray characteristics during the autoignition and subsequent combustion processes. After combining the experimental and modeling information, the following phases have been identified:

- I. *Non-reacting phase*, previous to autoignition, where the inert spray mixing process takes place.
- II. *Autoignition expansion phase*, where the spray volume first suddenly increases because of the onset of combustion. Axial expansion is not as important (max. $(S_r/S_i) \sim 1.05$) as in radial direction (max. $(\theta_r/\theta_i) \sim 2.7$). This phase is very short in time, and denotes the initial expansion of the reacting mixture due to the local drop in density.
- III. *Stabilization phase*, where the reacting tip penetration is similar to the inert case. If momentum is conserved, density drop due to combustion should result in a faster penetration of the spray. However, this is compensated by the strong initial increase in radial width. As a result, the reactive flow does not penetrate faster than the inert one.
- IV. *Acceleration phase*, where the reacting tip penetration progresses sensitively faster than the inert one, and eventually detaches from that of a non-reacting spray. During this period, the penetration ratio (S_r/S_i) increases steadily with time. According to the 1D model results, the flow evolution is trying to re-establish the initial momentum flux balance along the spray.
- V. *Quasi-steady flame phase*, where the axial penetration ratio (S_r/S_i) reaches a steady value. As a consequence, penetration evolution is similar to that of an inert spray, except for the faster rate of penetration due to the combustion-induced decrease in local density and the increase in radial expansion. For the investigated experiments, the stabilized (S_r/S_i) reaches a maximum value of 1.3, and has been observed to depend primarily on ambient temperature, i.e. flame local temperatures.

To the authors' knowledge, no systematic study on the spray tip evolution under reacting conditions has been published before. As reviewed in the introduction, no clear conclusions on the reacting tip behavior compared to the inert one were available. This is probably the main contribution of the present work, namely the previous definition of reacting spray phases. Furthermore, parametric variations have made it possible to verify that these phases always occur, but the particular duration extends when moving to less

reacting conditions (lower temperature or density) so that they may not even be observed within injection duration. Increasing either injection pressure or nozzle diameter also accelerates such processes, but visualization of such events is limited by window size, which in the present study was around 100mm. It must be noted that time scales for the observation of all these stages are usually very long compared to usual engine injection duration (within few microseconds). Furthermore, swirl effects, time-varying thermodynamic conditions due to piston movement and wall impingement will modify this picture when going to real engine conditions. However, the sequence of events makes an interesting picture for the description of spray-related processes during the injection-combustion sequence. A next step should be the comparison of these stages with the usual engine heat release rate ones. Spray tip evolution should also be investigated more deeply by means of detailed CFD simulations.

Acknowledgements

This work was partially funded by the Spanish Ministry of Science and Technology through the "EFFICIENT AND CLEAN COMBUSTION IN COMPRESSION IGNITION ENGINES USING THE DUAL-FUEL CONCEPT" project (TRA2011-26359). Mr. Francisco J. Briceño wishes to acknowledge financial support through a PhD studies grant (AP2008-02231) also sponsored by the Spanish Ministry of Education and Science. Last, but not least, authors would like to express their gratitude to José Enrique del Rey for his enthusiasm, proactiveness and help during data acquisition.

References

1. J.E. Dec, SAE Trans. 106 (3) (1997) 1319-1348.
2. M. Musculus, P. C. Miles, L. M. Pickett, Progress in Energy and Combustion Science 39 (2–3) (2013) 246-283, 2013.
3. D.L. Siebers, Transactions of the SAE 94 (1983) 673-686.
4. S. Matsuoka, T. Kamimoto, H. Kobayashi, SAE Paper 845009, 1984
5. V. Bermúdez, J. M. García-Oliver, E. Juliá, S. Martínez, SAE Paper, 2003-01-1110, 2003.
6. R. Payri, J. M. García-Oliver, M. Bardi, J. Manin, Applied Thermal Engineering 35 (2012), 185-195.
7. J. D. Naber, D. L. Siebers, SAE Paper 960034, 1996.
8. L. M. Pickett, J. Manin, C. Genzale, D. L. Siebers et al., SAE Int. J. Engines 4 (1) (2011) 764-799.
9. B. Higgins, D. L. Siebers, A. Aradi, SAE Paper 2000-01-0940, 2000.
10. B. Higgins, D. L. Siebers, SAE Paper 2001-01-0918, 2001.
11. D. L. Siebers, B. Higgins, SAE Paper 2001-01-0530, 2001.
12. L. M. Pickett, D. L. Siebers, Combustion and Flame 138 (2004) 114-135.
13. L. de Francqueville, G. Bruneaux, B. Thirouard, SAE Int. J. Engines 3 (1) (2010) 163-182.
14. F. Payri, J. V. Pastor, J. M. García-Oliver, J. M. Pastor, Meas. Sci. Technol 18 (2007) 2579-2598.
15. M. Musculus, L. M. Pickett, Combustion and Flame 141 (4) (2005) 371-391.
16. S. Kook, L. M. Pickett, Proceedings of the Combustion Institute 33(2) (2011) 2911-2918.
17. D.T. Hountalas, H. Ofner, G. Maragiannis, Thiesel 2006 Conference on Thermo- and Fluid Dynamic Processes in Diesel Engines, Sept. 12th to 15th, 2006.
18. H. Kobayashi, T. Kamimoto, S. Matsuoka. SAE Paper 810259, 1981.
19. D. L. Siebers. Chapter 5 in Flow and combustion in reciprocating engines. Springer-Verlag, 2009.
20. L. M. Pickett, L. Hoogterp. SAE Int. J. Commer. Veh. 1(1) (2009) 108-118.
21. J. M. Desantes, J. V. Pastor, J.M. García-Oliver, J. M. Pastor, Combustion and Flame 156 (2009) 234-249.
22. J. V. Pastor, J. J. López, J. M. García-Oliver, J. M. Pastor, Fuel 87 (2008) 2871-2885.
23. J. V. Pastor, R. Payri, J. M. García Oliver, F. J. Briceño, SAE Int. J. Engines 6(3) (2013) :1661-1676, .
24. G. S. Settles, Schlieren and shadowgraph techniques, Springer-Verlag, 2001.
25. J. V. Pastor, R. Payri, J. M. García Oliver, J. Nerva, SAE Paper 2012-01-0456, 2012.
26. B. Marciniak, M. Wysocki, *Infrared Phys. Technol* 51 (2008) 137-145.

27. <http://www.sandia.gov/ecn/dieselSprayCombustion.php> , last access on November 27th, 2013
28. <http://www.cmt.upv.es/ECN.aspx> , last access on November 27th, 2013
29. L. M. Pickett, C. Genzale, G. Bruneaux, L. Malbec et al., *SAE Int. J. Engines* 3 (2) (2010)156-181.
30. L.M. Pickett, S. Kook, T. Williams. *SAE Int. J. Engines* 2 (1) (2009) 439-459.
31. M. Bardi, R. Payri, L. M. Malbec, G. Bruneaux et al., *Atomization and Sprays* 22 (10) (2012) 807-842.
32. M. Musculus, K. Kattke, *SAE Int. J. Engines* 2(1) (2009)1170-1193, 2009.
33. J. Abraham, *Numerical Heat Transfer Part A*, 30: 347-364, 1996
34. D. Han, M.G. Mungal, *Combust. Flame* 124 (2001) 370-386
35. J. V. Pastor, R. Payri, J. M. García-Oliver, Francisco J. Briceño, *Atomization and Sprays* 21(6) (2011) 503-520.
36. L. M. Pickett, D. L. Siebers, C. A. Ichideria, *SAE Paper* 2005-01-3843, 2005.
37. F. Payri, J. V. Pastor, J. Nerva, J. M. García-Oliver, *SAE Int. J. Engines* 4 (2) (2011) 2278-2297.
38. E. Cenker, G. Bruneaux, L.M. Pickett, C. Schulz, *SAE Int. J. Engines* 6 (1) (2013) 352-365.

List of Symbols and Acronyms

SYMBOL	DEFINITION
CPF	Constant Pressure Flow
ECN	Engine Combustion Network
EGR	Exhaust Gas Recirculation
EOI	End Of Injection
ET	Energizing Time
LOL	Lift-Off Length
R	Detected spray radius
S	Spray penetration
T_{air}	Ambient temperature
X	Spatial coordinate along the spray axis
ϕ	Equivalence ratio
ρ_{air}	Ambient density
θ	Spray cone angle
d_{eq}	Equivalent diameter
d_0	Nozzle geometrical diameter
k	Proportionality constant
u_0	Injection velocity

List of Tables

Schlieren Camera	
Frame rate (fps)	47000
Exposure time (μs)	0.3
Image resolution (pixel)	544 x 184
mm-pixel ratio	0.297

Table 1. Recording set-up for schlieren imaging

<u>Ambient Conditions</u>	Bulk temperature (K)/density (kg/m ³)
NO	826, 21.2
HT	870, 21.2
LT	778, 21.2
HD	826, 28.4
LD	826, 17.2
Oxygen Concentration	0% (non-reacting) and 21% (reacting)
<u>Injection Settings</u>	
Fuel	n-heptane
Injector Type	Bosch Solenoid-activated
Nozzle Type	Mini-sac; Single Hole
Nozzle Diameter	82 μm and 138 μm
Nozzle Conicity	$K_{82}=1.5$; $K_{138}=2.9$
Energizing time	4 ms
Injection Pressure	50, 100 and 150 MPa
Injector Coolant Temperature	363 K

Table 2. Operating conditions

Parameters	U_0	T_{air}	ρ_{air}	d_0	R ² [%]	RMSE
Exponents	a	b	c	d	-	-
Pickett et al. OH*[36]	1	-3.74	-0.85	0.34	-	-
Payri et al. OH* [37]	0.88	-5.26	-0.75	-	-	-
All conditions in Table 2	0.72	-4.65	-1.09	0.25	94.09	1.09

Table 3. Schlieren lift-off model coefficients for the parametric study summarized in **Table 2**. OH* model coefficients found in literature are reported for comparison

List of figures

Figure 1. Schematic of the optical set-up for schlieren visualization

Figure 2. Instantaneous lift-off length definition reported in [23]. Time ASOI: 1787 μs . NO conditions in

Table 2. $\Delta P_{\text{inj}}= 50 \text{ MPa}$, nozzle diameter $d_0= 138 \mu\text{m}$.

Top: Reactive (red solid line) and fixed inert contours (yellow dashed lines).

Bottom: Detected contour and determination of the LOL from schlieren image

Figure 3. Composed time sequence of the spray penetration for both reacting (right-contour) and non-reacting (left-contour). HT conditions in **Table 2** $\Delta P_{\text{inj}} = 50\text{MPa}$, Nozzle diameter $d_0= 82 \mu\text{m}$.

Figure 4. Top: Temporal evolution of the penetration and lift-off length (LOL_S) from schlieren image processing for condition HT as described in section 5.1. **Bottom:** Temporal evolution of the axial penetration ratio (S_r/S_i). Nozzle diameter $d_0= 82 \mu\text{m}$.

Figure 5. Bottom: Temporal evolution of the expansion factor (θ_r/θ_i) for the HT reacting spray in **Figure 3. Top:** Overlaid inert (yellow) and reacting (red) least-squares fittings of cone angle.

Figure 6. Comparison between experiments and 1D spray model results of the inert and reacting spray tip penetration (top) and ratio of penetrations between the inert and reacting cases (bottom). Experimental conditions are the same as in **Figure 3**. Evolution of equivalence ratio on the spray axis for the inert spray (top, right) is also included to show the calculation of equivalence ratio at the Lift-Off Length ϕ_{LOL} .

Figure 7. Reacting spray behavior for a parametric variation of ΔP_{inj} . Temporal evolution of axial penetration (top) and radial expansion (bottom) ratios. Ambient temperature and density correspond to the HT condition in **Table 2**, 870 K and 21.2 kg/m^3 respectively; $d_0= 82 \mu\text{m}$.

Figure 8. Temporal evolution of axial penetration (top) and radial expansion (bottom) ratios. Parametric variation of air temperature. $\Delta P_{\text{inj}}= 50 \text{ MPa}$, $\rho_{\text{air}}=21.2 \text{ kg/m}^3$; $d_0= 82 \mu\text{m}$.

Figure 9. Temporal evolution of axial penetration (top) and radial expansion (bottom) ratios. Parametric variation of air density. $\Delta P_{\text{inj}}= 50 \text{ MPa}$, $T_{\text{air}}=870 \text{ K}$; $d_0= 82 \mu\text{m}$.

Figure 10. Temporal evolution of axial penetration (top) and radial expansion (bottom) ratios. Parametric variation of Nozzle diameter. $\Delta P_{\text{inj}}= 50 \text{ MPa}$, $T_{\text{air}}=870 \text{ K}$ and $\rho_{\text{air}}=21.2 \text{ Kg/m}^3$.

Appendix-A. Supplementary data

Supplementary data associated with this article can be found in the on-line version consisting of a video file showing the time-resolved schlieren visualization of both non-reacting and reacting sprays. For the HT operating conditions in *Table 2* composite images were created with half image of each spray, some of the images have also been shown in *Figure 3*. The video sequence exemplified the different stages of the reacting spray penetration that have been described in detail from *Figure 3* to *Figure 5*.

figure 1.tif

[Click here to download high resolution image](#)

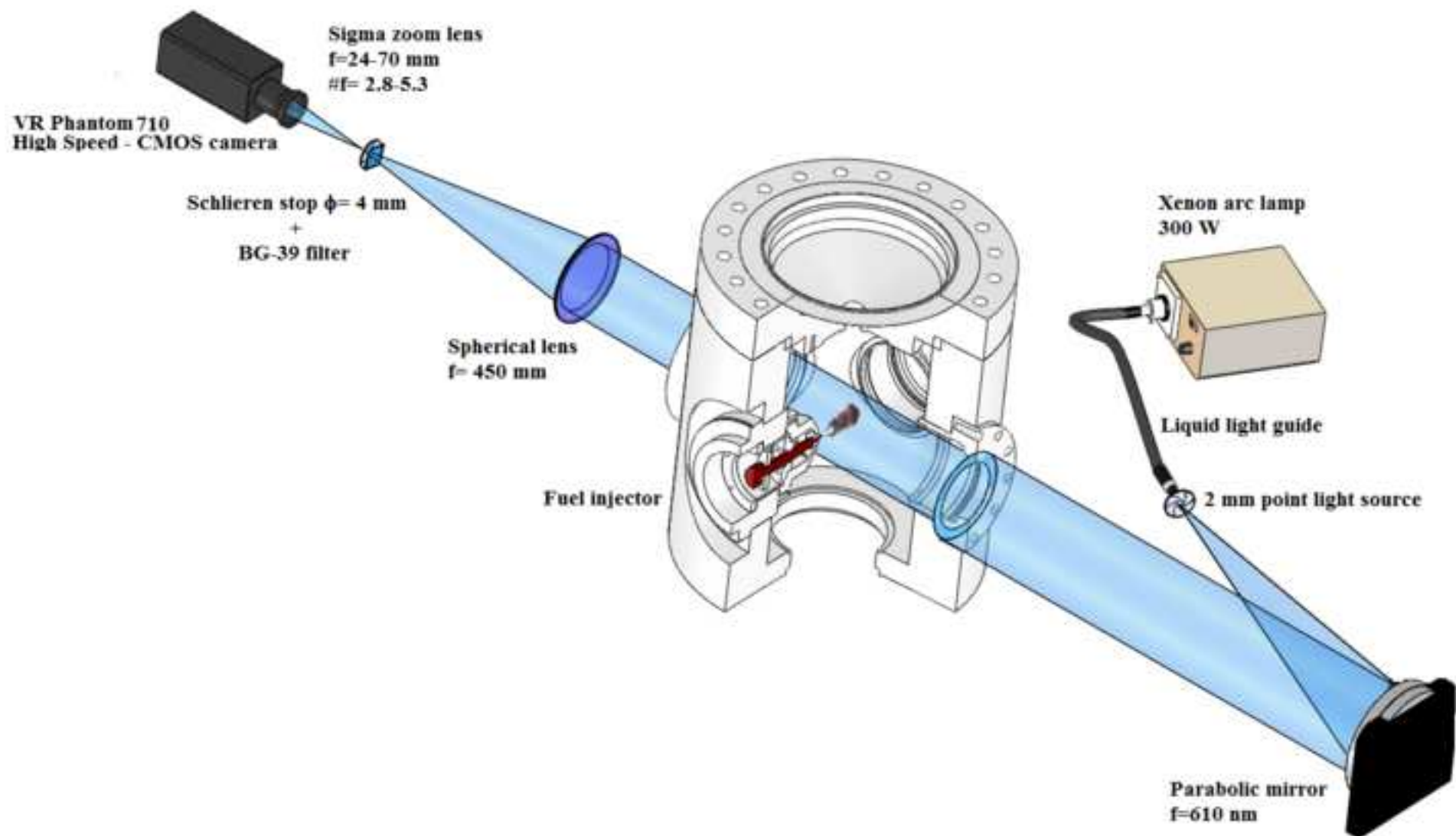


Figure 2.tif
[Click here to download high resolution image](#)

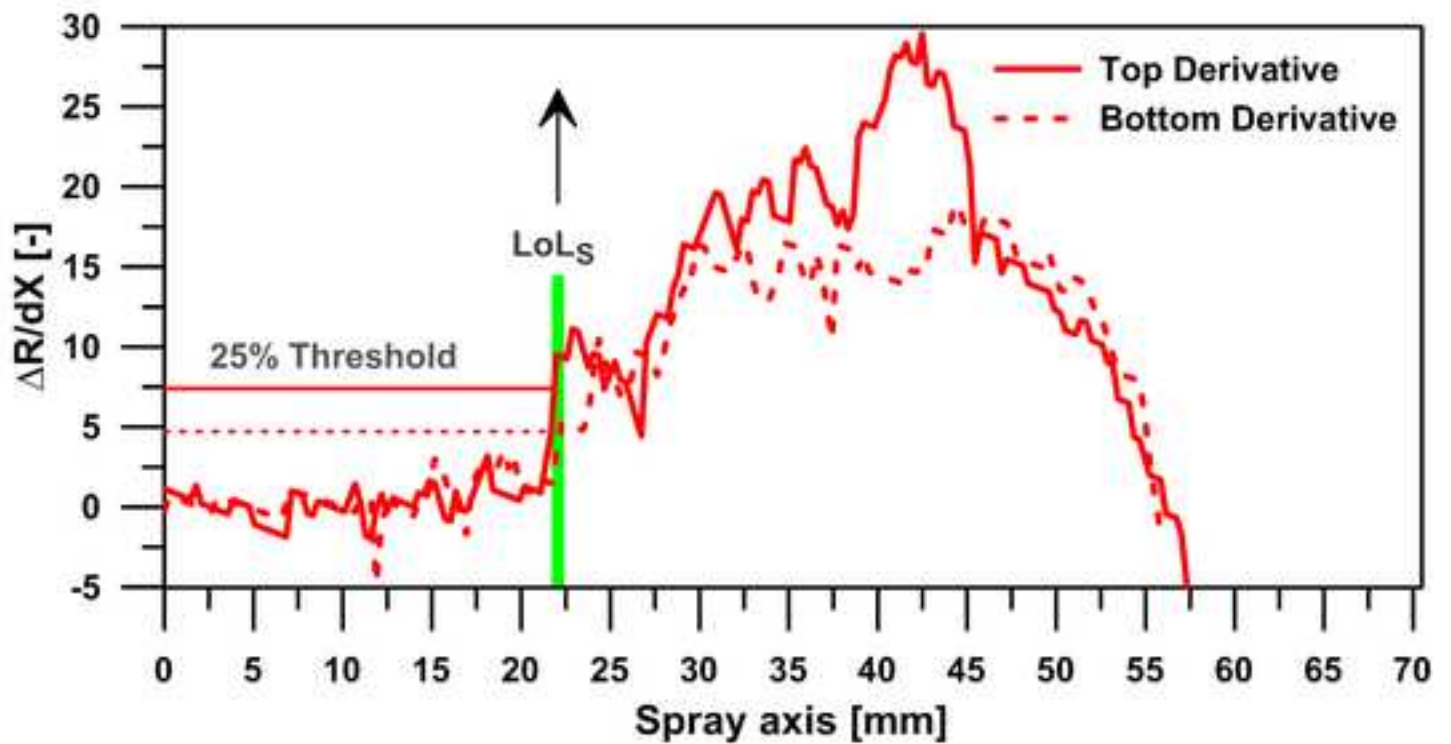
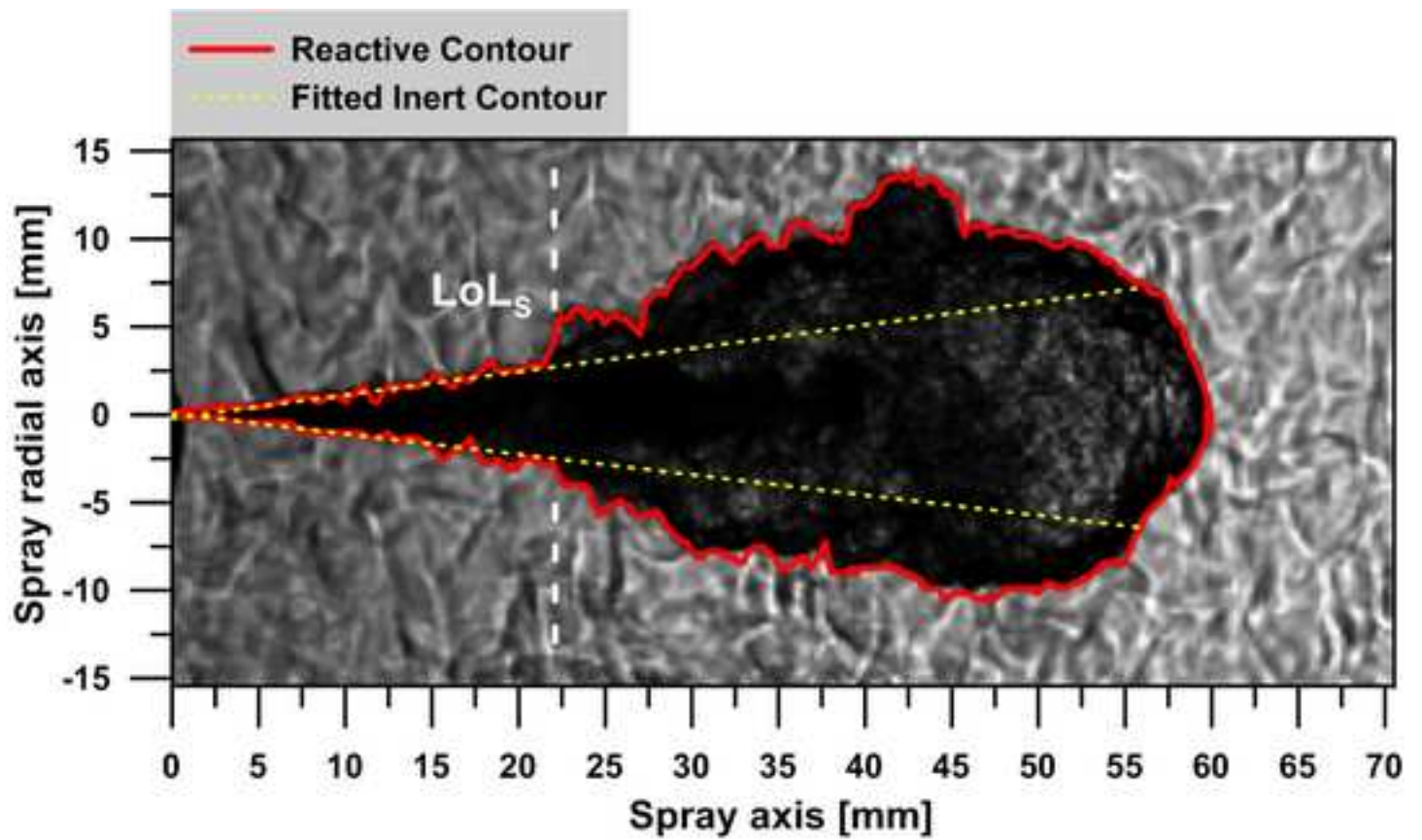


figure 3.tif
[Click here to download high resolution image](#)

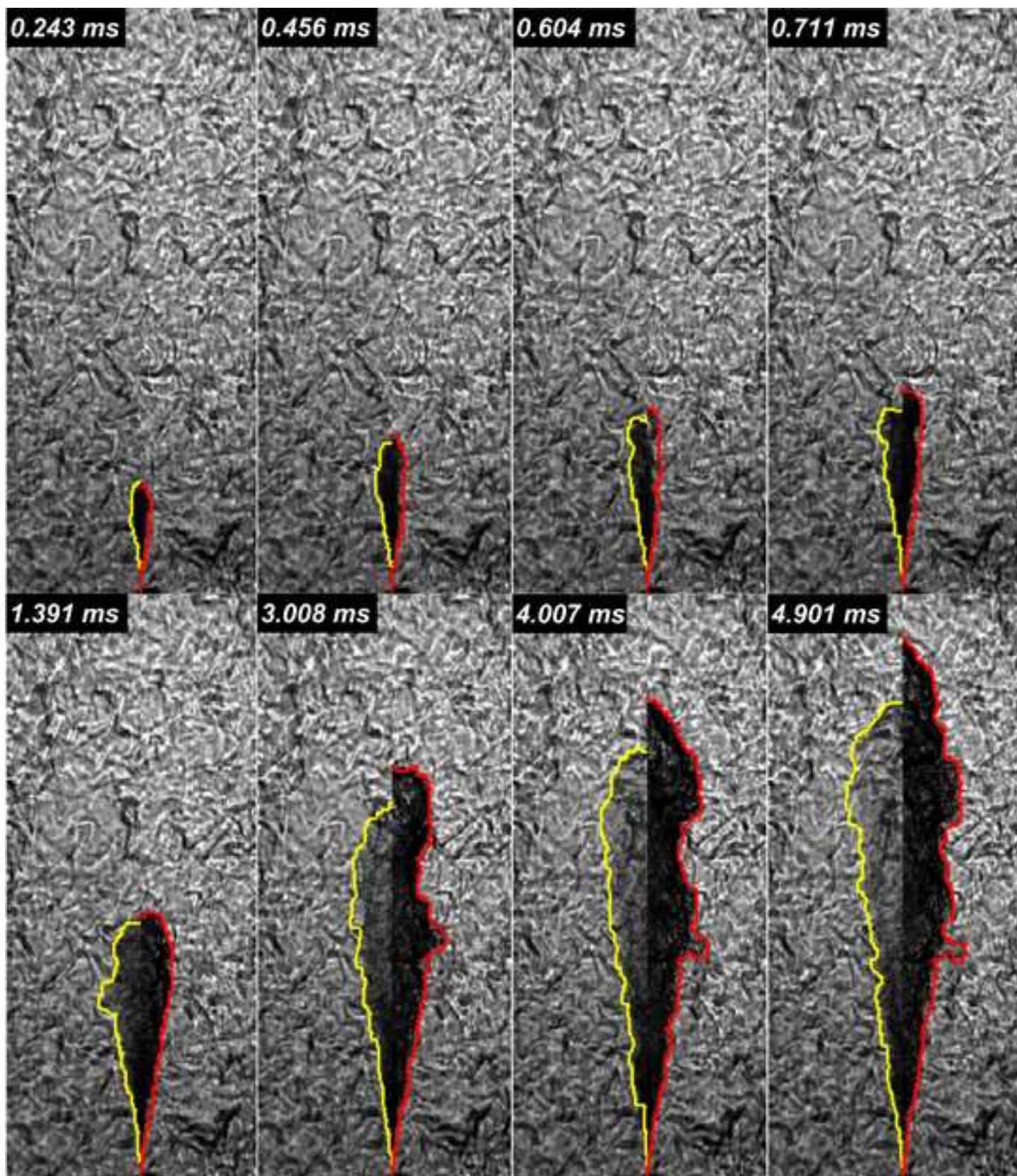


figure 4.tif
[Click here to download high resolution image](#)

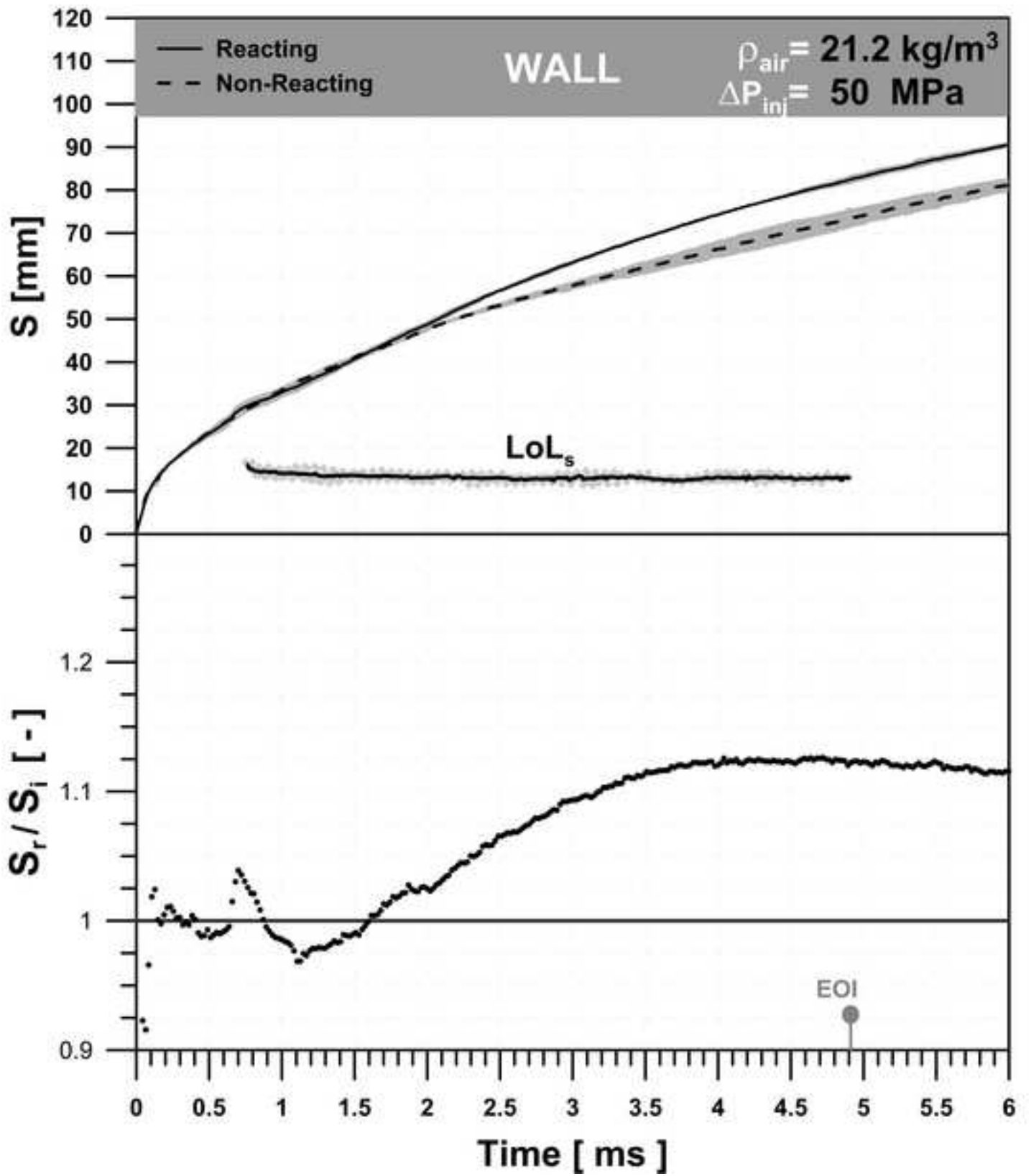


figure 5 bottom.tif
[Click here to download high resolution image](#)

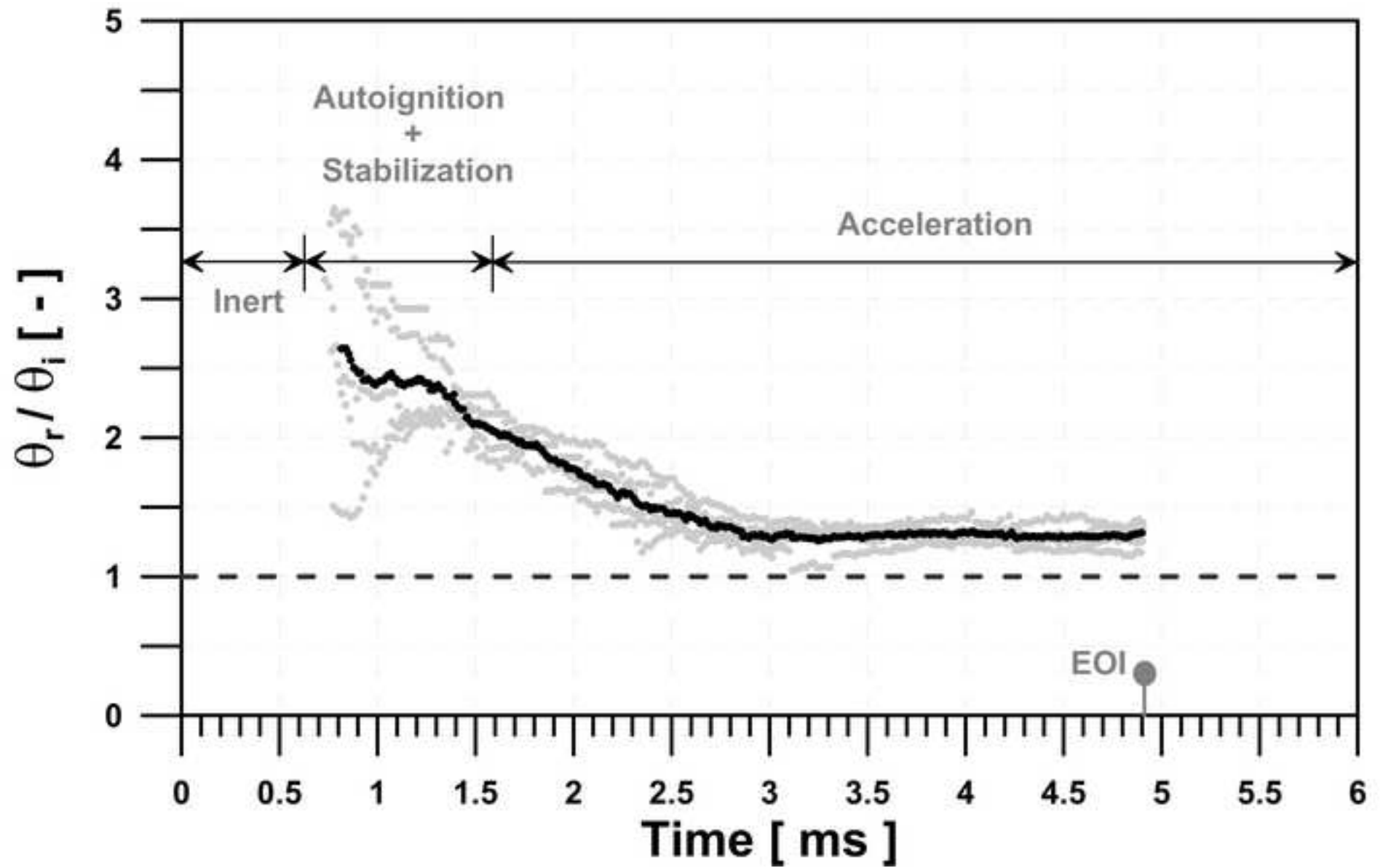


figure 5 top.tif
[Click here to download high resolution image](#)

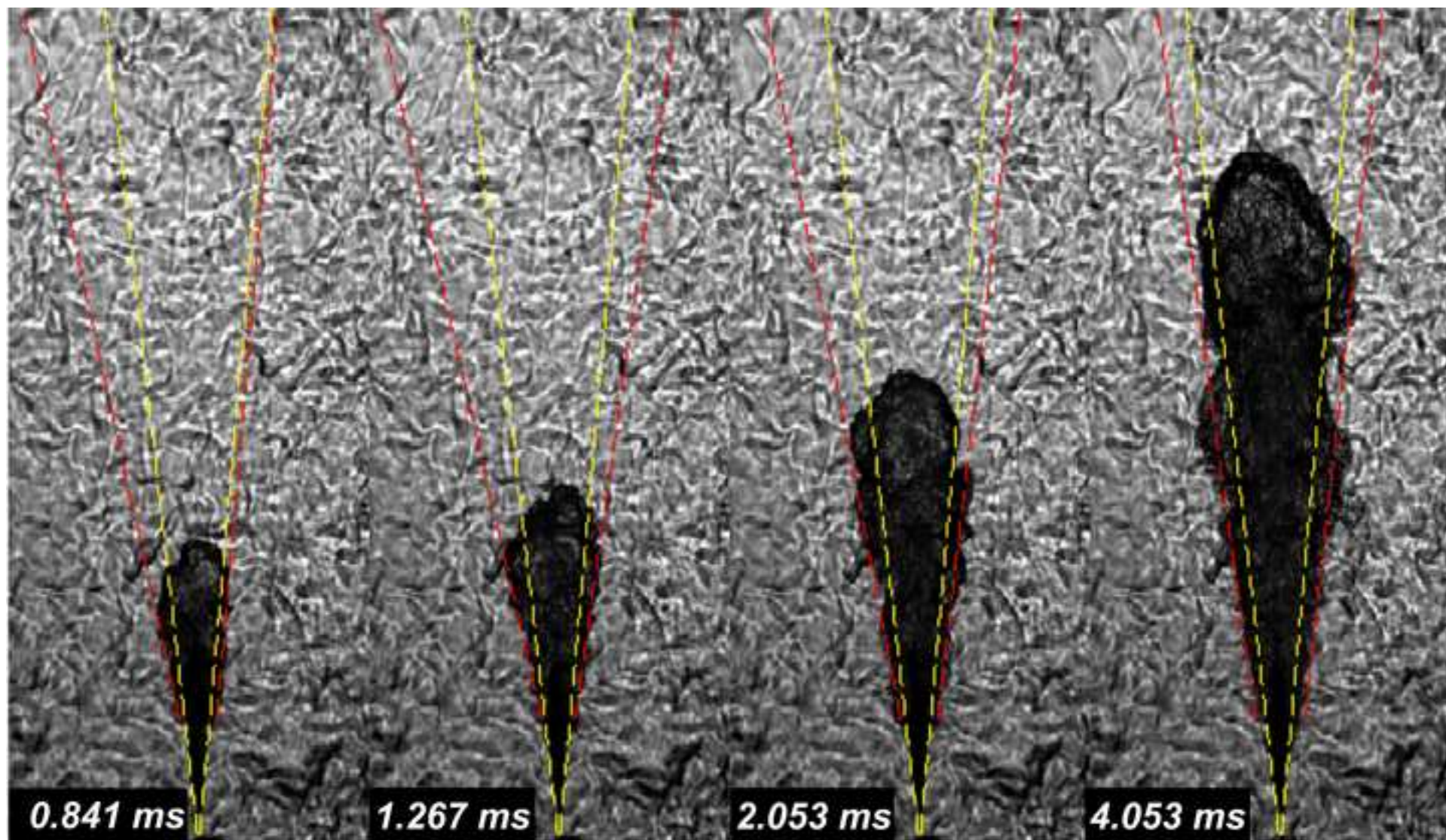


figure 6.tif

[Click here to download high resolution image](#)

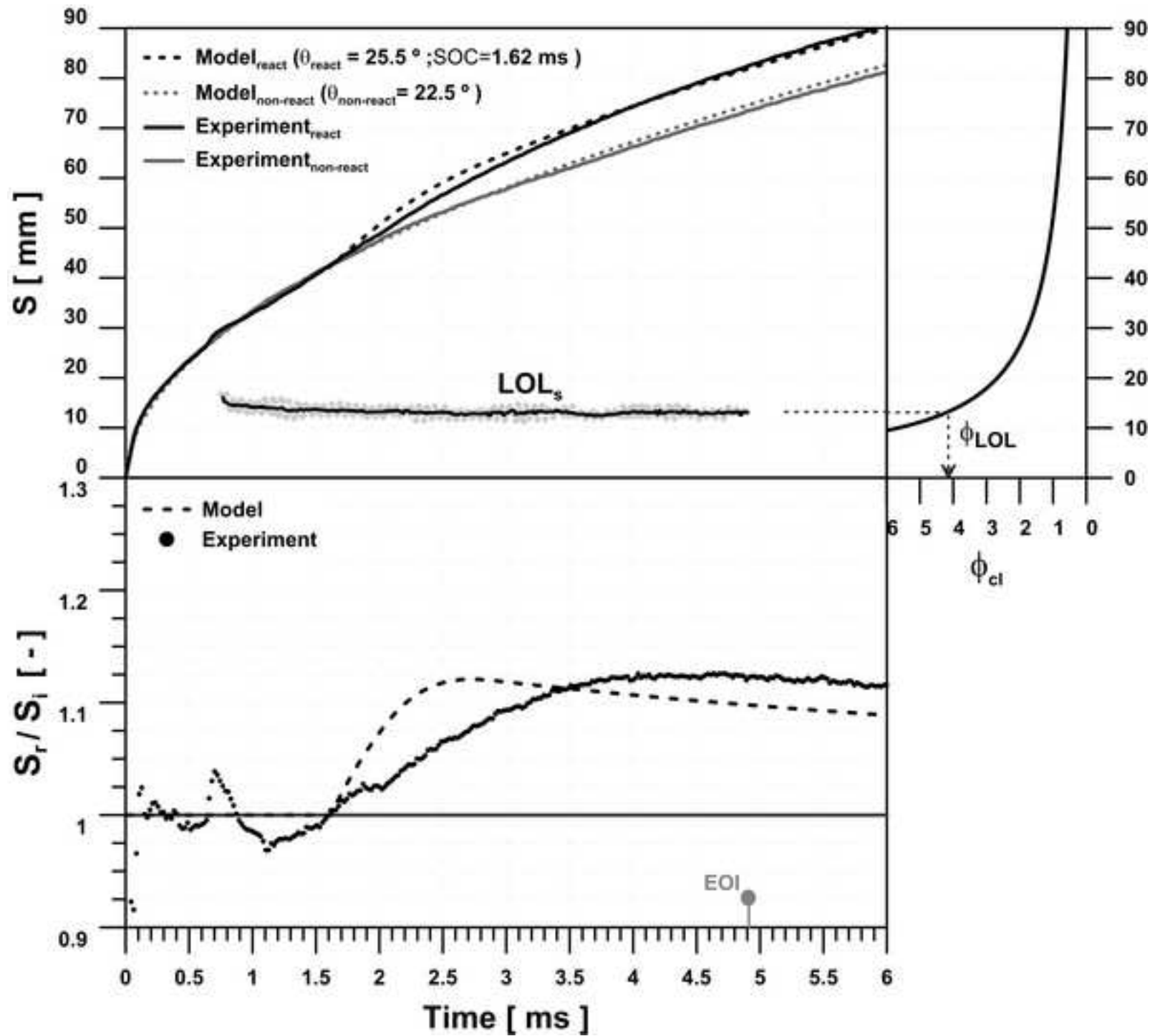


figure 7.tif
[Click here to download high resolution image](#)

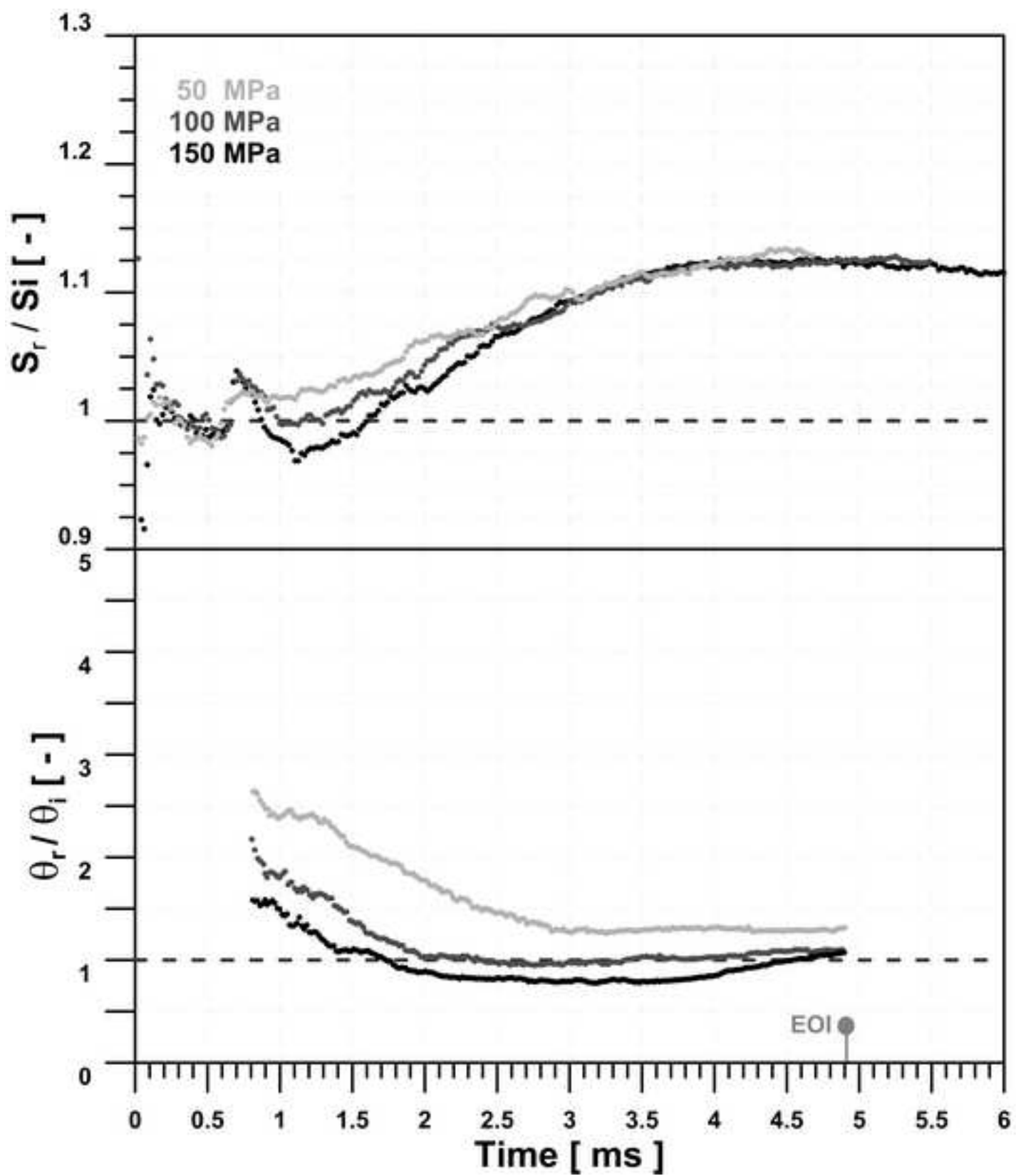


figure 8.tif
[Click here to download high resolution image](#)

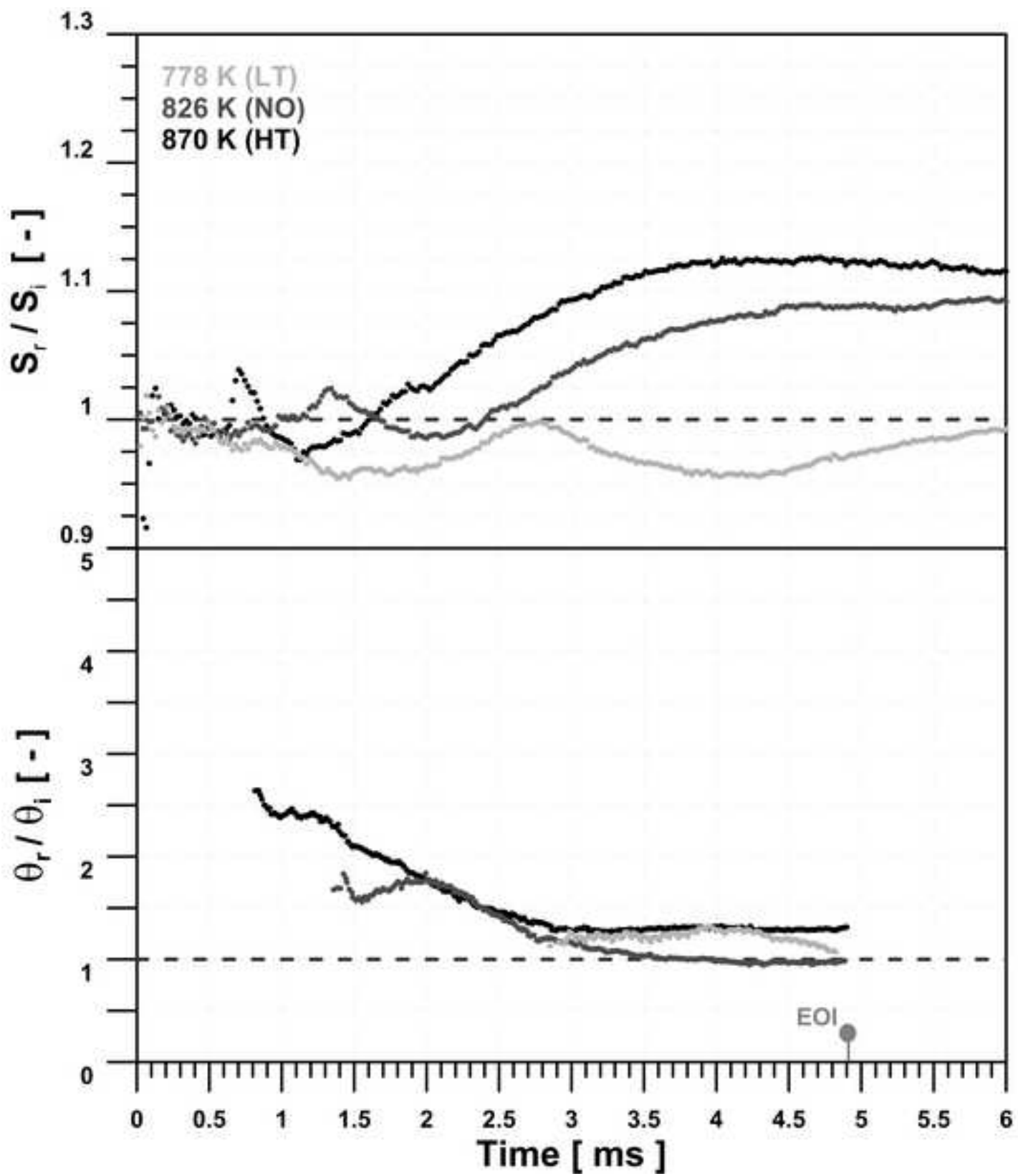


figure 9.tif
[Click here to download high resolution image](#)

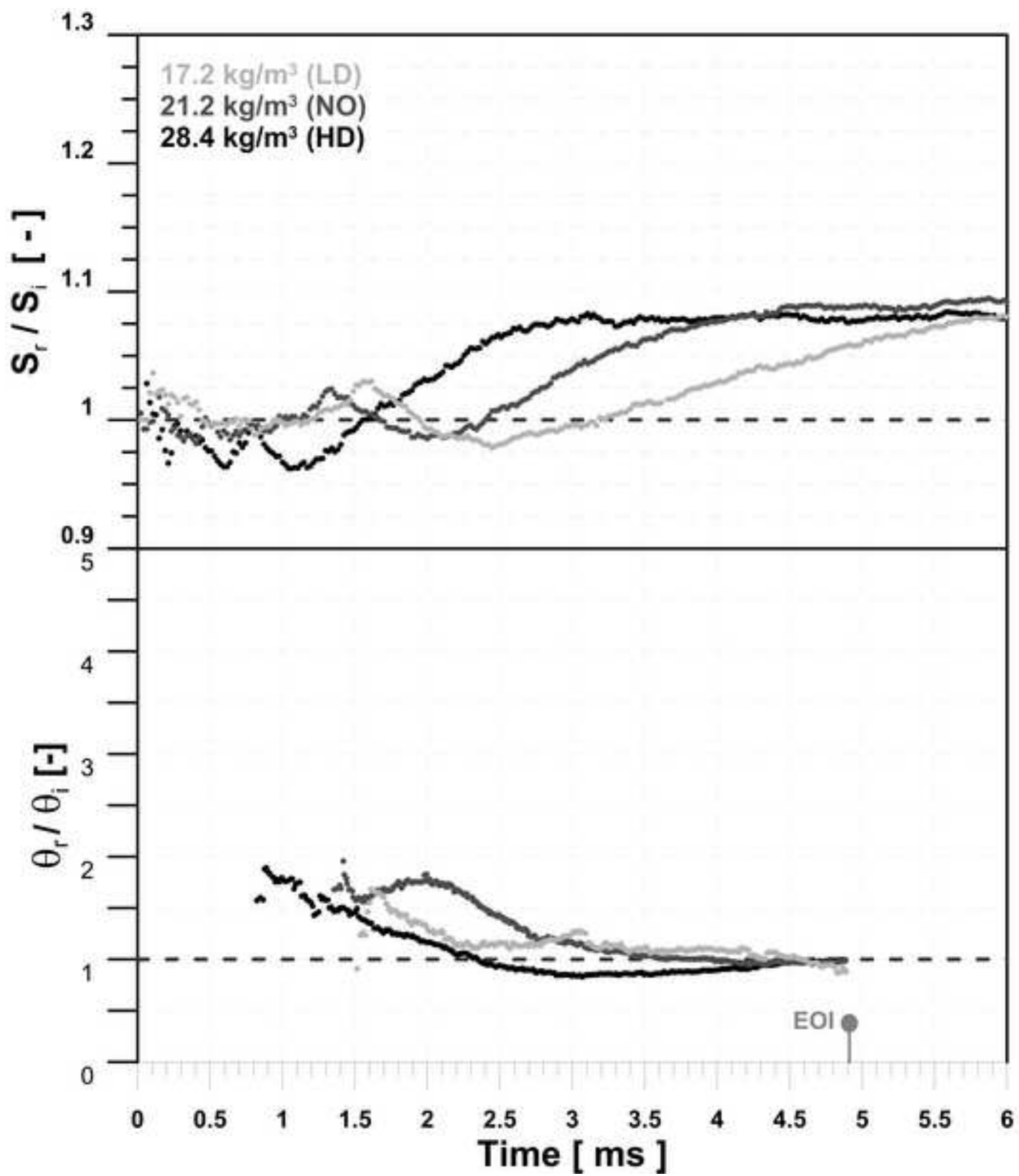
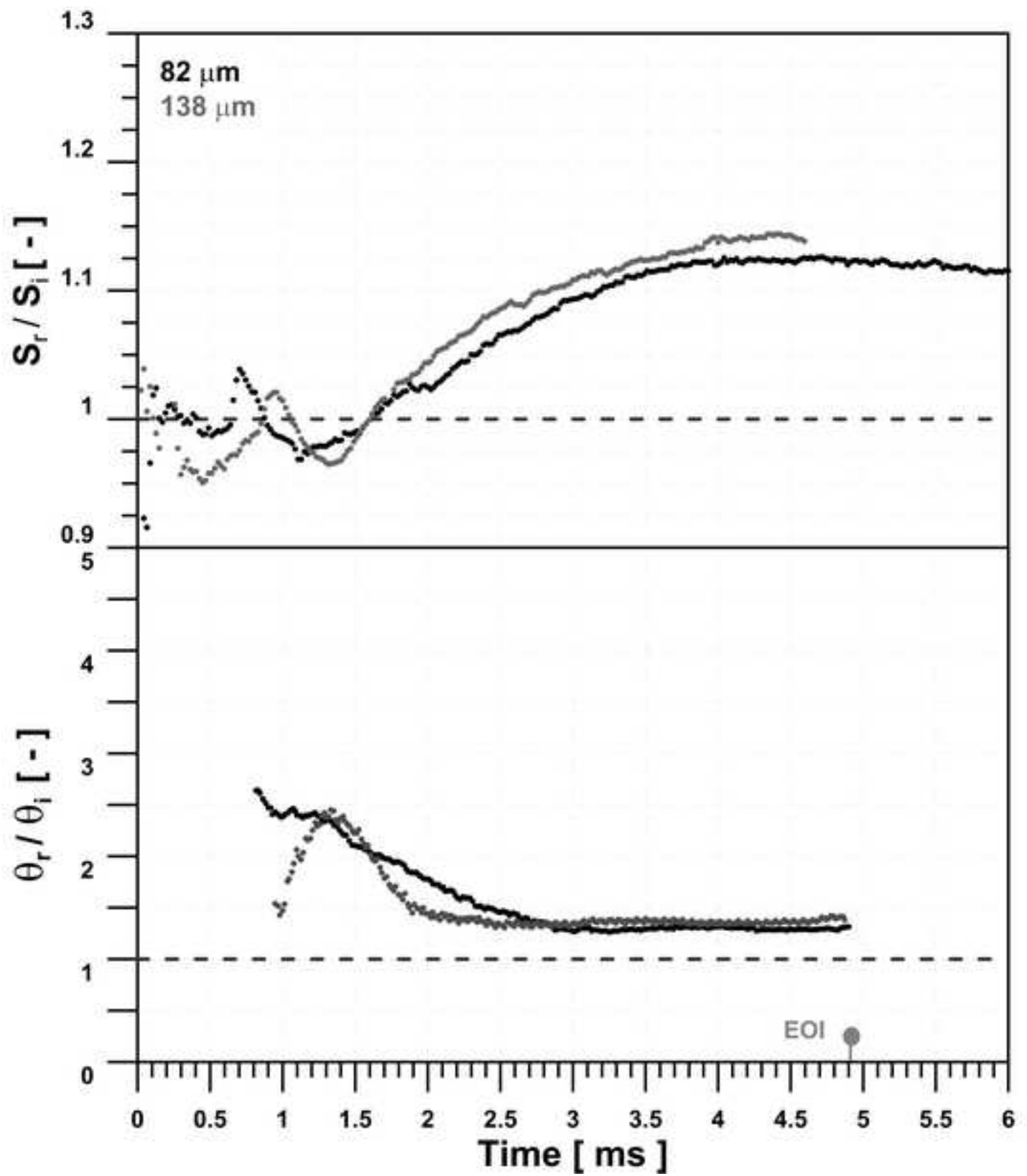


figure 10.tif
[Click here to download high resolution image](#)



This file could not be included in the PDF because the file type is not supported.